Supporting Information for

Functional Plastic Films: Nano-engineered Composite based Flexible Microwave Antennas with Near-unity Relative Visible Transmittance

Cheng Zhang[1], *, Liang Zhu[2], Chengang Ji[3], Zhilu Ye[2], Nabeel Alsaab[2], Minye Yang[2], Yuhui Hu[1], Pai-Yen Chen[2, *], and L. Jay Guo[3, *]

[1] School of Optical and Electronic Information & Wuhan National Laboratory for Optoelectronics, Huazhong University of Science and Technology, Wuhan, 430074, China

cheng.zhang@hust.edu.cn

[2] Department of Electrical and Computer Engineering, University of Illinois at Chicago, Chicago, IL 60607, USA

pychen@uic.edu

[3] Department of Electrical Engineering and Computer Science, University of Michigan, Ann Arbor, MI 48109, USA

guo@umich.edu

I. Simulated transmittance through a 7-nm-thick Cu-doped Ag film on PET substrate
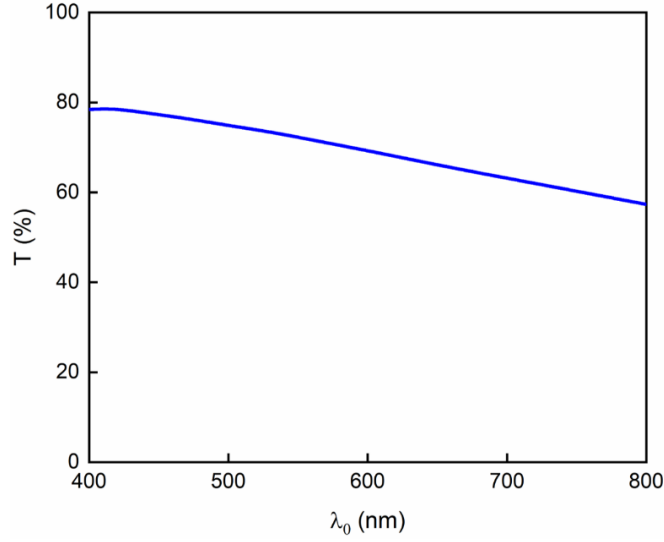

Figure S1. Simulated absolute transmittance spectrum over the visible region through a 7-nm-thick Cu-doped Ag film on PET substrate.

II. Numerical calculation of the resonant frequency of a planar dipole antenna

To obtain the resonant frequency of a planar dipole antenna, we commence by examining a cylindrical dipole antenna with a total length of $2L$ and a radius of a. Here, L represents the arm length of the dipole, and the separation gap g between the arms is disregarded since $g \ll L$. An empirical equation that correlates the dimensions of the dipole to its resonant frequency is given by:

$$2L = \frac{0.48cF}{f_r\sqrt{\varepsilon_{reff}}} \tag{S1}$$

where $F = L/(L + a)$, c is the free-space light speed, f_r is the resonant frequency, and ε_{reff} is the effective permittivity of the antenna substrate. When employing a substrate with a relative permittivity of ε_r, the effective permittivity can be written as:

$$\varepsilon_{reff} = \frac{\varepsilon_r + 1}{2} \tag{S2}$$

Here, we consider a planar dipole with length of $2L$ and width of w. The equivalence between the width w of a planar dipole and the radius a of a cylindrical dipole can be expressed as:

$$w = 4a \tag{S3}$$

Based on the above analysis, the resonant frequency of a planar dipole antenna can be expressed as:

$$f_r = \frac{0.96c}{(4L + w)}\sqrt{\frac{2}{1 + \varepsilon_r}} \tag{S4}$$

III. Characterisation of nanocomposite-based dipole antennas at 2.0 GHz and 4.2 GHz

Figure S2 plots the characterised radiation patterns of the $D_{2.0}$ OTA on the E- and H-planes, showing a maximal realised gain of -0.45$\pm$0.12 dBi. Its radiation performance is similar to dipole antennas made of opaque materials such as Ag ink (denoted by the blue lines) and Cu paste (denoted by the black lines).
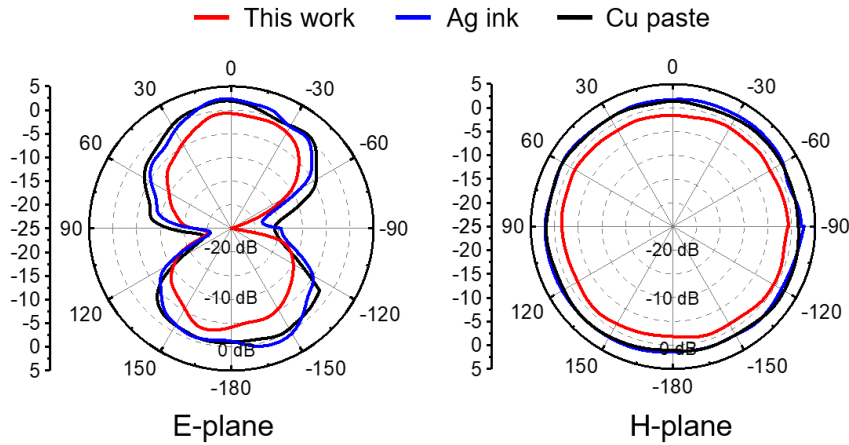

Figure S2. Measured realised gain as a function of observation angle (radiation pattern) on the E-plane (left panel) and H-plane (right panel) for three 2.0 GHz dipole antennas, whose arms are respectively made of the proposed nanocomposites (red lines), silver ink (blue lines), and copper paste (black lines).

Figure S3 plots the characterised radiation patterns of the $D_{4.2}$ OTA on the E- and H-planes, showing a maximal realised gain of -1.15$\pm$0.32 dBi. Its radiation performance is similar to dipole antennas made of opaque materials such as Ag ink (denoted by the blue lines) and Cu paste (denoted by the black lines).
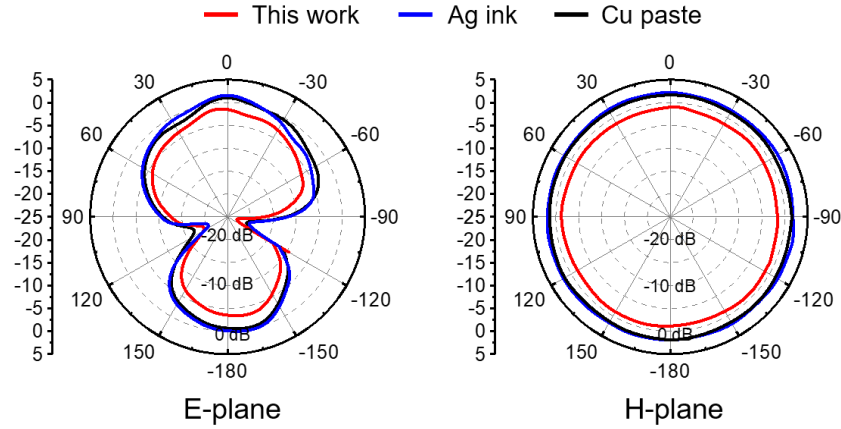
Figure S3. Measured realised gain as a function of observation angle (radiation pattern) on the *E*-plane (left panel) and *H*-plane (right panel) for three 4.2 GHz dipole antennas, whose arms are respectively made of the proposed nanocomposites (red lines), silver ink (blue lines), and copper paste (black lines).

IV. Performance of the nanocomposite-based flexible dipole antenna after cyclic bending

Figure S4 shows the reflection coefficients of a flexible dipole antenna with varying bending cycles, demonstrating the robust performance of the antenna after cyclic bending. The results are obtained from Ansys High Frequency Simulation Software (HFSS). During the simulation, we take into account the sheet resistance of the nanocomposite structure after bending cycles (displayed in Fig. 1e of the main text), which is the primary factor that affects the performance of the antenna.
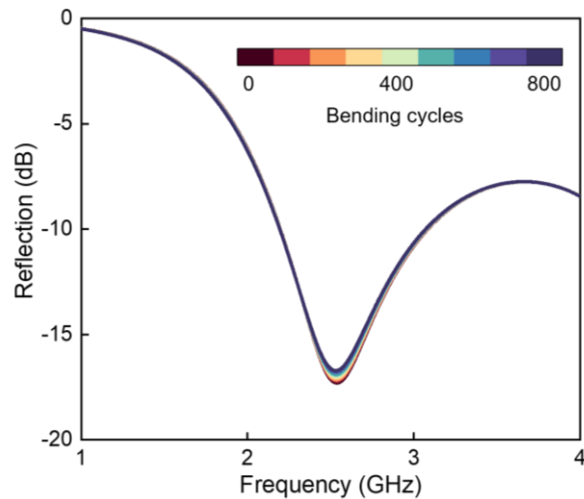

Figure S4. Simulated reflection coefficients of the flexible dipole transparent dipole antenna with different bending cycles.

V. Geometric parameters of the high-gain Yagi-Uda OTA

The geometric parameters of the transparent high-gain Yagi-Uda OTA are listed in Table S1.

Table S1. Geometric parameters of the transparent high-gain Yagi-Uda OTA in this study.

Parameter	L_1	L_2	L_3	w_1	w_2	w_3	d_1
Value (mm)	35	40	48	12	12	12	16

VI. Geometric parameters of the transparent microstrip patch OTAs

The geometric parameters of the transparent microstrip patch OTAs are listed in Table S2.

Table S2. Geometric parameters of the transparent microstrip patch OTAs in this study.

OTA	L (mm)	w (mm)
$P_{5.8}$	15	10.8
$P_{6.5}$	13.2	10.8
$P_{8.2}$	10.5	7.5

VII. Numerical calculation of the resonant frequency of a microstrip patch antenna

A microstrip antenna is composed of a rectangular patch with a physical length of L and width of w, and a ground plane, which are spatially separated by a dielectric substrate with a height of h. Due to the fringing effect, the electrical dimensions of the patch along its length appear to be larger than its physical dimensions. Specifically, the length of the patch is extended on both ends, resulting in an effective length of $L_{eff} = L + 2\Delta L$. The extension of the length can be expressed as:

$$\Delta L = 0.412h \frac{\left(\varepsilon_{eff} + 0.3\right)\left(\frac{w}{h} + 0.264\right)}{\left(\varepsilon_{eff} - 0.258\right)\left(\frac{w}{h} + 0.8\right)} \tag{S5}$$

The effective permittivity ε_{eff}, which takes into account the impact of fringing, is a parameter introduced for describing wave propagation in the microstrip. On condition that $w/h > 1$, the effective permittivity is given by:

$$\varepsilon_{reff} = \frac{\varepsilon_r + 1}{2} + \frac{\varepsilon_r - 1}{2}\left[1 + 12\frac{h}{w}\right]^{-\frac{1}{2}} \tag{S6}$$

where ε_r is the relative permittivity of the dielectric substrate. The resonant frequency of a microstrip patch antenna for the dominant TM$_{100}$ mode can thus be written as:

$$f_r = \frac{1}{2L_{eff}\sqrt{\varepsilon_{reff}}\sqrt{\mu_0\varepsilon_0}} = \frac{1}{2(L+2\Delta L)\sqrt{\varepsilon_{reff}}\sqrt{\mu_0\varepsilon_0}} \tag{S7}$$

where μ_0 and ε_0 are the permeability and permittivity of vacuum, respectively. For an efficient radiator, a practical width of the patch that leads to an optimized radiation efficiency is given by:

$$w = \frac{1}{2f_r\sqrt{\mu_0\varepsilon_0}}\sqrt{\frac{2}{\varepsilon_r+1}} = \frac{c}{2f_r}\sqrt{\frac{2}{\varepsilon_r+1}} \tag{S8}$$

VIII. Spectroscopic ellipsometry characterisation of the deposited films

The film's refractive index and thickness value are characterised by reflection-mode spectroscopic ellipsometry using the interference enhancement method, at three different angles of incidence (55°, 65°, and 75°) with respect to the normal to the substrate plane. During the Cu-doped Ag film deposition, we place a calibration substrate into the deposition chamber together with the real samples. The calibration substrate is a silicon wafer with a ~ 300 nm thermal oxide layer. After the film deposition, we further check thickness of the deposited film by characterising the calibration substrate through spectroscopic ellipsometry using the interference enhancement method. After the film thickness is obtained by spectroscopic ellipsometry, we can further analyze the fitting error as a function of Cu-doped Ag thickness. There will be a minimum/converging fitting error at ~ 7 nm (Fig. S5), which is consistent with predicted thickness based on the pre-calibrated deposition rate and serves as direct evidence of the ultra-thin feature of the deposited film.
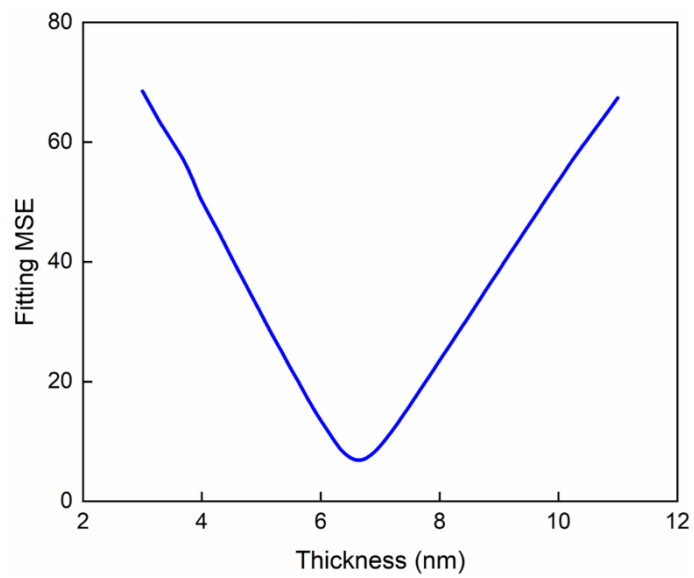
Figure S5. Fitting MSE of the thickness value of the deposited Cu-doped Ag film during the spectroscopic ellipsometry characterisation.